Time-Domain Modelling of Pulsed Photoconducting Sources - Part I
The Norton Equivalent Circuit

Neto, Andrea; Juan, Nuria Llombart; Freni, Angelo

DOI
10.1109/TAP.2022.3184517

Publication date
2023

Document Version
Final published version

Published in
IEEE Transactions on Antennas and Propagation

Time-Domain Modelling of Pulsed Photoconducting Sources—Part I: The Norton Equivalent Circuit

Andrea Neto, *Fellow, IEEE*, Nuria Llombart Juan, *Fellow, IEEE*, and Angelo Freni, *Senior Member, IEEE*

***Abstract*— In the circuit theory, the Norton and Thevenin equivalent generators are tools that simplify the solutions of networks involving passive or active components. They have been extensively used in the frequency domain to describe time-harmonic sources. A time-stepped evolution is instead typically used to include transient sources. As a particular case of the latter, the Norton equivalent circuit is extended here to investigate pulsed photoconducting sources, where a dc bias voltage and a pulsed optical laser are combined to generate terahertz (THz) bursts. The proposed derivation relies on the application of the electromagnetic (EM) equivalence theorem. The main conclusion of this derivation is the understanding that, from the three different spectral regions (dc, THz, and optics), only the THz radiation is to be explicitly included in the equivalent circuit. The theory is validated by a campaign of measurements reported in a connected paper.**

***Index Terms*— Equivalence theorem, Norton equivalent circuit, photoconductive (PC) sources.**

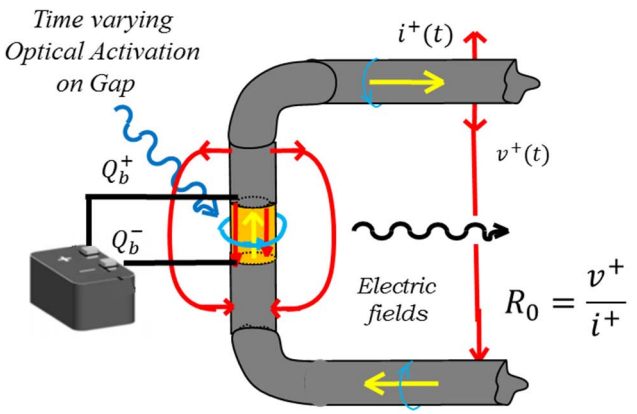

Fig. 1. Schematic connection between a PC source and a TEM transmission line.

I. Introduction

THE development of sources in high-frequency systems requires the close integration between active and passive components. A family of devices that has been receiving increasing attention over the last decades is pulsed photoconductive (PC) terahertz (THz) sources [1]–[5]. Their modeling, however, is particularly challenging. One of the challenges is that three types of signals, the bias, the laser activation, and the generated harmonic components in the THz spectrum, converge and interact on the same semiconductor gap, schematically shown in Fig. 1. The most widely accepted modeling of these structures is probably emerging from the work in [6] that presented equivalent circuits with components at these different frequencies. However, the equivalent circuits shown in [6] presented an additional screening generator. The parameters of this screening generator were experimentally tuned to match the measurement but could not be predicted. After [6], only minor modifications of the representations emerged. A review of various equivalent circuits proposed in the literature can be found in [7].

An approximate Norton equivalent circuit, with a single equivalent generator in the THz spectrum, has been introduced in [8] for the characterization of the radiation of PC antennas (PCAs). The approximate circuit was derived in the frequency domain, introducing a time-averaged generator resistance. However, when used for the characterization of sources with significant power, in the order of the tens of microwatts, the approximate equivalent circuit in [8] proved to be not accurate [9]. The goal of this article is to derive a rigorous, time-domain (TD), single generator, equivalent Norton circuit that can replace the frequency-domain constant resistance in [8] with a component that accurately represents the time evolution of the PC source.

TD circuits have been used routinely in the past for the analysis of transients in circuits that include active devices. Researchers from Bell's Laboratory proposed in 1968 [10] to investigate separately the linear and nonlinear domains and to solve the interface in the TD. However, such a procedure was never used in the study of pulsed PC sources and is presented here for the first time. This article explicitly focuses on a Norton circuit. The circuit is shown to be a direct consequence of the application of the equivalence theorem in electromagnetism. An equivalent surface is used to separate an internal and an external portion of the source, in correspondence with the device terminals. Since the objective is the characterization of the THz source spectrum, the equivalence theorem

Manuscript received 15 September 2021; revised 14 February 2022; accepted 4 April 2022. Date of publication 24 June 2022; date of current version 6 March 2023. *(Corresponding author: Andrea Neto.)*

Andrea Neto and Nuria Llombart Juan are with the THz Sensing Group, Microelectronics Department, Delft University of Technology, 2628 CD Delft, The Netherlands (e-mail: a.neto@tudelft.nl).

Angelo Freni is with the Dipartimento di Ingegneria dell'Informazione, University of Florence, 50121 Florence, Italy.

Color versions of one or more figures in this article are available at https://doi.org/10.1109/TAP.2022.3184517.

Digital Object Identifier 10.1109/TAP.2022.3184517

currents are chosen to represent, in TD, only the THz harmonics of the field. The separate treatment of the mentioned THz harmonics is the main insight that is clarified in this article.

After its derivation, the Norton circuit is applied to calculate the current and voltage drop on a typical PC source. These voltage and currents provide a direct estimation of the power radiated by the source as well as its spectral distribution. A representative time evolution of the source, including the bias, is obtained and thus used to estimate the THz energy provided by the source, which includes the ohmic losses. The procedure clarifies that the generated available THz power is, for instance, the one launched in the infinite transmission line shown in Fig. 1. The energy associated with the THz pulse, radiated and dissipated, is all initially stored in the dc bias. The dc energy is converted into THz energy by the activated gap only after enabling from the laser pulse. Thus, an energy transformation efficiency can be defined as the ratio between the energy available to the load acting in the THz spectrum and the total energy provided by the dc battery bias. This is in contrast with the main assessment, in both the physics [11] and antenna communities [12], that the qualifying PC source efficiency relates the THz energy to the optical power. As there are no accurate tools that can directly validate the present derivation, the results of this analysis are compared with measurements in [13].

This article is structured as follows. In Section II, a brief reminder of the basic mechanisms of pulsed PCAs is presented. In Section III, an integral equation representing the continuity of the tangent magnetic field is set up. It involves the presence of an assigned magnetic field and two scattered fields. In Section IV, these three contributions are evaluated and expressed in terms of the voltage across the load and the net current flowing in the source leading to the actual Norton equivalent circuit that can be used to solve for the voltage and the current that are actually estimated for in Section V. In Section VI, the energy considerations that lead to the introduction of an appropriate bias efficiency are provided. Finally, conclusions are drawn in Section VII.

II. Basic Mechanism of Photoconducting Sources

To clarify the basic steps of the procedure and the possibility to facilitate its extension to different geometrical realizations, the present investigation addresses a cylindrical canonical structure.

A. Biased Cylindrical Gap

A cylindrical volume V bounded by a surface S (see Fig. 2) is assumed to contain the biased PC material and receive the time-varying optical activation. The cylindrical structure is taken of length Δ_z and circular cross section of radius a. As an example, in Fig. 2(a), the red arrows depict a biasing (dc) electric field configuration, $\vec{e}_b = e_b(x, y)\hat{z}$. When a time-varying optical excitation frees several electrons that can move in the bulk material, an electric current density $\vec{j}(\vec{r}, t)$ will flow in V [yellow arrows in Fig. 2(b)].

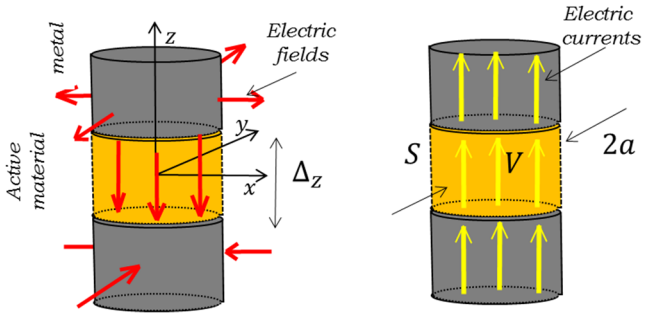

Fig. 2. (a) Biasing electric field, red lines, in the finite PC volume. (b) Electric currents in the presence of optical excitation, yellow lines.

Outside the active volume, the polarization of the electric field is orthogonal to the conductive contours (shown in gray in Fig. 2). In the following, the cylinder volume V will be assumed to be very small in terms of the dc and THz wavelengths so that the net current, $i(t)$, in the gap is assumed to be constant with respect to z and to be the flux of the distribution $\vec{j}(\vec{r}, t)$ over any the cross section of the cylinder. Also, a voltage can be defined as the integration of the electric field between the small cylinder bases. The PC source is electrically connected to a load so that the generated electromagnetic (EM) energy is available to the user. In the following, the load will be assumed to be a matched transmission line characterized by a known characteristic impedance R_0 at high frequencies (THz). However, it can be assumed that at low frequencies, dc, the load is an open circuit. The connection to the transmission line is schematically represented in Fig. 1. We assume that the transmission line does not alter the cylindrical symmetry of the field close to the source.

B. Time Evolutions

The time evolution of the voltage and current in pulsed PC sources is fairly well described in the literature, see [12]. EM waves distributed upon three different spectral regions coexist in the same device: the dc bias, the THz, and the optical.

With reference to Fig. 1, a continuous voltage bias V_b is applied across the load gap where the PC material is located. In this contribution, the dc biasing is assumed to be a voltage, V_b, constant in time, as sketched in Fig. 3(a). A train of optical pulses $p_{opt}(t)$ with repetition period T impinges on the PC gap [see Fig. 3(b)]. Each optical pulse lasts τ_p seconds and frees electrons from the valence band into the conduction band, allowing the movements of the electrons accumulated in the metal of the gap, and thus, a time-varying current $i(t)$ [see Fig. 3(c)] can flow. The current pulse lasts roughly τ_c (recombination time) seconds, which is the time constant before the electrons and the holes recombine and is characterized by $\tau_p \ll \tau_c \ll T$. The amplitude of the optical activation defines the number of free charges, but their speed and direction are a result of the bias voltage. The PC material is activated in the tens of femtoseconds scale (τ_p) by the optical pulses and the metallic pads are then discharged in sub-picosecond time scales ($\approx\tau_c$). Because

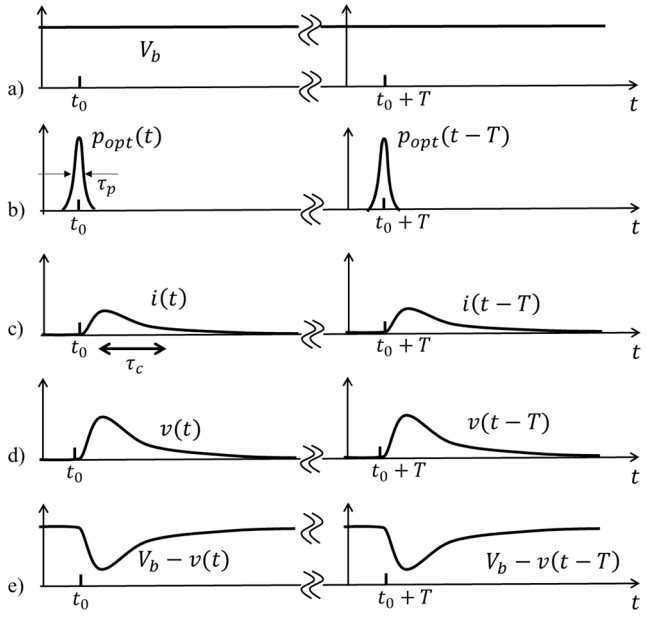

Fig. 3. Time evolution of currents and voltages on the gap for two successive periods. (a) DC bias, (b) optical power pulses, (c) transient current, (d) transient voltage on the load, and (e) total voltage on the gap.

of this rapid material response, the current generates a THz pulse that propagates along the transmission line of Fig. 1. This generation represents the desired available THz power and the transmission line represents the load R_0. The PC material is characterized by high resistivity when not excited, and thus, the electric current during the pulses, $t \in (0, \tau_c)$, can be approximated as the only current in the gap and the load. The metallic pads, i.e., cylindrical bases also visible in Fig. 1, behave as a capacitor discharged and then charged on comparable time scales (τ_c). With the discharge and charge, there is a corresponding rapid voltage swing, $v(t)$, across the gap [see Fig. 3(d)]. The voltage generated by the pulses, $v(t)$, opposes the bias electric field since it is in response to the movement of the free charges. Thus, the complete voltage across the gap can be expressed as $v_g(t) = V_b - v(t)$ [see Fig. 3(e)]. This qualitative description of the time evolution of voltages and currents neglects a detailed analysis of the impact that the specific implementation of the bias circuitry has on the recharge time. In fact, the transient voltages across the capacitor of the gap could be slightly different from zero also in the absence of currents in the PC gap. However, this effect will be neglected throughout this work, as it does not contribute to the generation of THz field components.

C. Instantaneous Power

The instantaneous power generated at the cylindrical gap that is available to the THz load can be expressed as follows:

$$p_l(t) = v(t)i(t). \tag{1}$$

Since the load is reactive at extremely low frequencies in any real structure of finite length, the dc voltage does not contribute to the desired THz power generation, $p_l(t)$. The dc voltage component V_b must be retained to evaluate the undesired power dissipated in the gap itself due to the finite conductivity of the PC material. This power can be expressed as follows:

$$p_{diss}(t) = [V_b - v(t)]i(t). \tag{2}$$

Accordingly, the total energy provided by the source fuels both the desired transmission in the load, p_l, and the undesired ohmic losses, p_{diss}. The total power can be expressed as the sum of these two components. The mobile electrons $i(t)$ freed by the optical power host both mechanisms since it appears that

$$p_{tot}(t) = p_{diss}(t) + p_l(t) = V_b i(t). \tag{3}$$

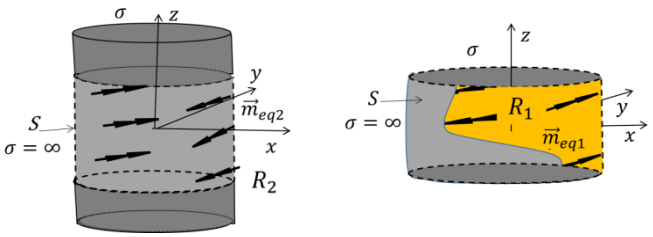

Fig. 4. Magnetic equivalent currents backed by PEC at the interface between a source (region 1) which is assumed small in terms of the wavelength, and the free space (region 2). The schematic representation includes the equivalent currents for region 1 (right) and the ones for region 2 (left).

III. Norton Circuit via the Integral Equation for Magnetic Field Continuity

To be able to predict the feedback effect of the loading of the line on the source, both the source and the exterior problem (i.e., the transmission line) must be solved simultaneously, addressing a very large domain. This procedure would be demanding for any numerical multiphysics tool that would have to rely on a fine-time discretization as well as a fine spatial discretization of the domain of analysis. In the next few sections, we will derive a rigorous Norton equivalent circuit in TD that will allow to solve for $i(t)$, $v(t)$. Due to the separation of the source and the load in the formulation, in the future, the circuit will be able to solve more complex problems than the simple one in Fig. 1.

To derive rigorously the equivalent circuit for a source, one must solve Maxwell's equations subject to specific boundary conditions. A common procedure is to apply the equivalence theorem [14] and to solve for the unknown equivalent currents via an integral equation. The choice of the form of the equivalence theorem dictates which currents, electric, magnetic, or both, must be selected. In turn, the type of currents dictates if the resulting equivalent circuit is Thevenin-like (electric currents) or Norton-like (magnetic currents). A procedure to separate the problem of the source (R_1) from the surrounding (R_2) was presented for the first time in 1966 by Van Bladel [15], for a different application.

A. Equivalence Theorem With Perfect Electric Conductor

Applying the equivalence theorem to the cylindrical volume V in Fig. 4(a), the field scattered in the region external (R_2)

and internal (R_1) to the volume V can be equivalently represented as the field radiated by equivalent currents, distributed on the surface S that envelopes the volume V. The two regions can be separated by metallizing the surface $S$with a perfect electric conductor [14]. Since the equivalent currents radiate in the presence of the perfect electric conductor, only equivalent magnetic currents, $\vec{m}_{eq,i}$, with $i = 1, 2$ (see Fig. 4), are now contributing. They can be expressed in terms of the total time-varying electric field $\vec{e}$ at the interface $\vec{r} \in S$ as follows:

$$\vec{m}_{eq,i}(t, \vec{r}) = \vec{e}(t, \vec{r}) \times \hat{n}_i \tag{4}$$

with $\hat{n}_i$ the unit vector orthogonal to the surface S and pointing at the region R_i. The total magnetic field in R_2 is only the field $\vec{h}_{2,s}(\vec{r}, t)$, scattered by these currents. It can be calculated via Green's function that includes the presence of a metallic cylinder [see Fig. 4(a)]. The magnetic field in R_1 can instead be represented as the superposition of incident and scattered magnetic fields as follows:

$$\vec{h}_1(\vec{r}, t) = \vec{h}_{1,inc}(\vec{r}, t) + \vec{h}_{1,s}(\vec{r}, t). \tag{5}$$

The incident magnetic field, $\vec{h}_{1,inc}$, is the field generated inside the closed cylindrical cavity [see Fig. 4(b)] by the biasing voltage V_b, and therefore, it is also a function dependent on the bias: $\vec{h}_{1,inc}(\vec{r}, t, V_b)$. The biasing voltage, V_b, does not contain time-varying components; however, since the laser pulses modulate the constitutive relations of the material, $\vec{h}_{1,inc}(\vec{r}, t, V_b)$ is a THz modulated magnetic field. For this reason, later, it will be found more appropriate (10c) to indicate the related electric current as impressed current rather than an incident current. The scattered magnetic field, $\vec{h}_{1,s}(\vec{r}, t,)$, is radiated by the equivalent currents $\vec{m}_{eq1}$, in the presence of the closed cavity entirely filled by the PC source material and bounded by its metallic bases and the metalized surface S; therefore, in the following, we will explicitly show this dependence as $\vec{h}_{1,s}(\vec{r}, t, \vec{m}_{eq1})$. Moreover, $\vec{h}_{2,s} = \vec{h}_{2,s}(\vec{r}, t, \vec{m}_{eq2})$.

To find the unknown magnetic currents, one needs to impose the continuity of the tangential component of the magnetic field at the interface S between the two regions. Therefore, one can impose that for $\vec{r} \in S$

$$\hat{\rho} \times \left[\vec{h}_{1,inc}(\vec{r}, t, V_b) + \vec{h}_{1,s}(\vec{r}, t, \vec{m}_{eq1})\right] = \hat{\rho} \times \vec{h}_{2,s}(\vec{r}, t, \vec{m}_{eq2}). \tag{6}$$

Equation (6) represents an integral equation, where the unknowns are the magnetic currents $\vec{m}_{eq1}$ and $\vec{m}_{eq2}$. The continuity of the tangent components of the electric fields at the interface S is guaranteed by letting $-\vec{m}_{eq1} = \vec{m}_{eq2}$ since $\hat{n}_1 = -\hat{n}_2$. This implies that an integral equation in terms of a single unknown, $-\vec{m}_{eq1} = \vec{m}_{eq2} = \vec{m}_{eq}$, can be obtained

$$\hat{\rho} \times \vec{h}_{1,inc}(\vec{r}, t, V_b) = \hat{\rho} \times \left[\vec{h}_{1,s}(\vec{r}, t, \vec{m}_{eq}) + \vec{h}_{2,s}(\vec{r}, t, \vec{m}_{eq})\right]. \tag{7}$$

B. Electrically Small Cylindrical Structure

With the reference system chosen in Fig. 2, the directions in which both the electric fields and the electric currents are aligned on the surface S are $\pm\hat{z}$. From the electric fields in Fig. 2, one can extrapolate that the equivalent magnetic currents tangent to the surface S are directed along $\hat{\phi}$. Moreover, assuming $\Delta_z \ll \lambda$,[1] with λ the wavelength in the bulk's PC material at all frequencies investigated, and considering a cylindrical reference system (ρ, ϕ, z), one can approximate the time-varying electric field in the volume V as $\vec{e}(\vec{r}, t) = \hat{z}v(\rho, t)/\Delta_z$, where $v(\rho, t)$ is the voltage drop associated with the electric field. Considering also the radius of the cylinder $a \ll \lambda$, the voltage can also be assumed independent of ρ so that $v(\rho, t) \approx v(t)$ can be interpreted as a voltage drop. The equivalent magnetic currents in R_2, being independent of ϕ, can be expressed as follows:

$$\vec{m}_{eq}(\rho = a, \phi, z, t) = \frac{v(t)}{\Delta_z}\text{rect}\left(\frac{z}{\Delta_z}\right)\hat{\phi} \tag{8}$$

where $\text{rect}(x) = 1$ for all $|x| < 1/2$ and zero elsewhere. The net current in the cylinder can also be related to the magnetic fields tangent to the surface S. In fact, for cylinders small in terms of wavelength, $\vec{h}_{1,inc}(a^-, \phi)$, $\vec{h}_{1,s}(a^-, \phi)$, and $\vec{h}_{2,s}(a^+, \phi)$ are all oriented along $\hat{\phi}$ and independent of ϕ. Thus, the evaluation of the circulation along $\rho = a$ of the magnetic fields appearing in (7) can be read as follows:

$$i_{inc}(t, V_b) = i_{s1}(t, v) + i_{s2}(t, v). \tag{9}$$

One can note that the scattered currents i_{s1} and i_{s2} add up in (9) once they are both expressed in terms of $v(t)$. Equation (9) expresses the continuity of the tangent electric and magnetic fields as the continuity of the current in a node, see Fig. 5. To adopt a notation typically found in the formulations of the Norton theorem, one can define the current in the load, the internal current in the source, and the impressed current as follows:

$$i(t, v) \equiv i_{s2}(t, v) \tag{10a}$$

$$i_{int}(t, v) \equiv i_{s1}(t, v) \tag{10b}$$

$$i_{impr}(t, V_b) \equiv i_{inc}(t, V_b). \tag{10c}$$

IV. Evaluation of the Norton Circuit Components

The three terms appearing in (10) can be calculated for the specific case of a PC material excited by an optical pulse train.

A. Impressed Currents

The evaluation of the impressed current, $i_{impr}(t, V_b)$, requires the knowledge of the magnetic field corresponding to the incidence problem described in Fig. 6. In particular, Fig. 6 shows the metallic cavity and the dc bias electric field lines: $\vec{e}_b \approx {}^{V_b}/_{\Delta z}$. As a result of the low conductivity of the PC material before optical activation, no electric current is flowing for $t < t_0$. For $t > t_0$, a pulsed optical activation signal $p_{opt}(t, t_0, \tau)$ changes the property of the excited portion of photosensitive bulk material, on which the laser is focused. The electric current i_{inc} in (10c) can be thought of as the flux

[1] If we take, for example, LT GaAS with a dielectric constant of 12.9, the wavelength in the dielectric at 1 THz is about 0.083 mm. A typical volume of the PC source could be $\Delta_x \times \Delta_y \times \Delta_z = 10 \times 2 \times 10\ \mu\text{m}^3$. Since $\Delta_z = 10\ \mu\text{m} \cong \lambda/8$, the assumption is justified.

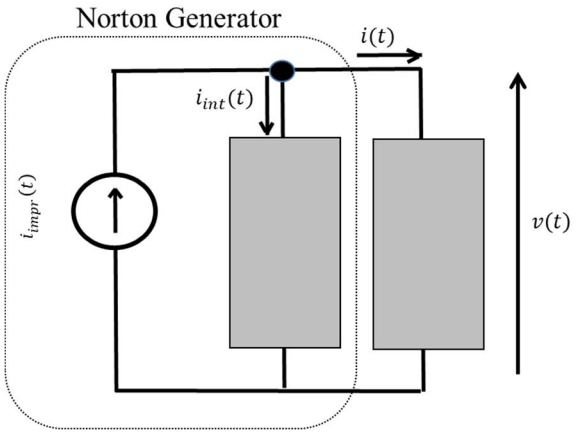

Fig. 5. Equivalent Norton circuit emerging as the continuity of the current at the node. This corresponds to impose the continuity of tangent components of the magnetic field at the boundary S of the cylinder in Fig. 4.

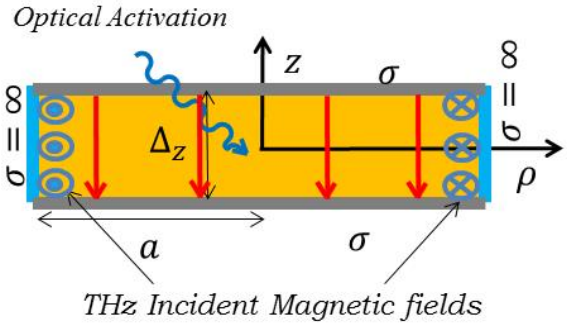

Fig. 6. Incident magnetic field at the boundary of the source region.

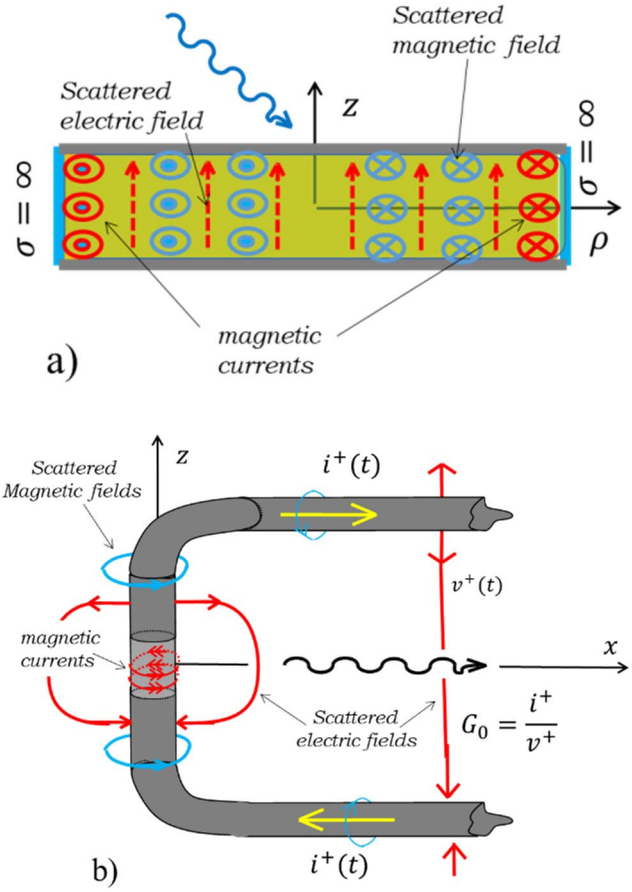

Fig. 7. Configurations pertinent to (a) inner and (b) outer scattered fields.

over the cylindrical cross section of a current density, $\vec{j}_{inc}(\vec{r}, t)$, that is related to the electric field in the PC material by the constitutive relation of a space invariant material. Since the cavity is small in terms of the wavelength, the time-dependent portion of the incident electric field is negligible, and therefore, $\vec{j}_{inc}(\vec{r}, t) \propto \vec{e}_b$ and does not depend on ρ. Accordingly, the constitutive relation can be expressed compactly as follows:

$$\vec{j}_{inc}(\vec{r}, t) = \hat{z} I_F^{je}\left\{t, \frac{V_b}{\Delta z}, t_0, p_{opt}\right\} = \hat{z}\int_{-\infty}^{t} F^{je}\left\{\frac{V_b}{\Delta z}, t_0, p_{opt}\right\} dt' \quad (11)$$

for $\vec{r} \in V$ and zero elsewhere. Here, the operator I_F^{je} represents a convolution function of the impulse response of the gap, dependent on the optical excitation power p_{opt} and the time t_0 at which it begins. The general expression of F^{je} for PC material is given in [16]. The parameters of this expression are provided in [13] for the special case of low-temperature (LT) gallium arsenide (GaAs).

Using (10c), the flux of the current density can be expressed as follows:

$$i_{impr}(t) = 2\pi \int_0^a I_F^{je}\left\{t, \frac{V_b}{\Delta_z}, t_0, p_{opt}\right\} \rho d\rho. \quad (12)$$

Finally, defining I_F^{iv} as a voltage–current constitutive relation dependent on the impulse response of the gap, we have

$$i_{impr}(t) = I_F^{iv}\left\{t, V_b, t_0, p_{opt}\right\} \quad (13)$$

where

$$I_F^{iv} \equiv \frac{\pi a^2}{\Delta_z} \vec{I}_F^{je}. \quad (14)$$

It is worth noting that $i_{impr}(t)$ presents THz harmonics even if it is associated only to the electric field associated with the bias voltage (V_b).

One could argue that a biasing electric field, $\vec{e}_b$, different from zero at locations tangent to the PEC boundaries at $\rho = a$, does not make sense. One should then realize that the equivalence theorem is applied only to the THz components of the EM field, and thus, the biasing electric field is unaffected. Effectively, this could be realized with a PEC metallization of the surface S that does not cover the entirety of the surface S. A small aperture between the top plates of the cylinder and the lateral PEC metallization could be maintained so that the electric dc electric field is not short-circuited.

B. Inner Scattered Fields

The EM problem giving rise to the scattered magnetic field and currents in R_1 is sketched in Fig. 7(a). Imposing

the constitutive relationship in (13) between the time-varying voltage $v(t)$ in the cavity and the corresponding current $i_{int}(t)$ leads to

$$i_{int}(t) = I_F^{iv}\{t, v(t), t_0, p_{opt}\}. \tag{15}$$

C. Outer Scattered Field

Finally, the geometry corresponding to Green's function required by the equivalence theorem for R_2 is sketched in Fig. 7(b). When the external circuit is represented by a conductance, $G_0 = 1/R_0$, of a TEM transmission line, the relationship between the voltage and the current in the load is simply a direct ratio

$$i(t) = v(t)G_0. \tag{16}$$

For a general type of load, the impulsive response of the load, $g_l^{imp}(t)$, needs to be used so that

$$i(t) = \int_{-\infty}^{t} v(t')g_l^{imp}(t-t')dt'. \tag{17}$$

V. Norton Circuit in TD

Equations (13), (15), and (17) provide the explicit values for the components of the circuit in Fig. 5, as reported in Fig. 8. Imposing the continuity of the current, we can write an equation for the current flowing in the load that must be verified for t > t_0 as follows:

$$i_{impr}(t) - i_{int}(t) = i(t) \tag{18}$$

or explicitly

$$\int_{-\infty}^{t} F^{iv}\{V_b - v(t'), t_0, p_{opt}dt' = \int_{-\infty}^{t} v(t')g_l^{imp}(t-t')dt'. \tag{19}$$

A. Solution of the Continuity Equation

Equation (19) can be solved numerically with a time-stepped evolution method. In particular, it can be obtained by expanding the voltage $v(t)$ in terms of subdomain basis functions. Many expansions are possible with some more efficient than others. Here, it was decided to use the simplest expansion possible, resorting to piecewise constant functions as follows:

$$v(t) \cong \sum_{n=-\infty}^{\infty} v_n \text{rect}[(t-t_n)/\delta t] \tag{20}$$

where $v_n = v(t_n)$, with $t_n = n\delta t - \delta t/2$, and the interval δt is assumed sufficiently small, with respect to the time scales associated with the problem, so that $v(t)$ can be considered constant in the subdomains. The described piecewise-constant temporal expansion of (20), even if it may not minimize the numerical effort, leads to correct solutions provided that one uses a high discretization step. Substituting (20) into (19), we obtain

$$\int_{-\infty}^{t} F^{iv}\left\{V_b - \sum_{n=-\infty}^{m} v_n \text{rect}\left[(t'-t_n)/\delta t\right]\right\}dt' = \int_{-\infty}^{t} \sum_{n=-\infty}^{m} v_n \text{rect}\left[(t'-t_n)/\delta t\right] g_l^{imp}(t-t')dt' \tag{21}$$

where the summations are extended to the index m, which identifies the time interval associated with the observation time $t \in [t_m, t_m + \delta t]$. For the linearity of the problem, (21) can be discretized as follows:

$$\sum_{n=-\infty}^{m} I_{m,n}^{s} = \sum_{n=-\infty}^{m} v_n I_{m,n}^{imp} \tag{22}$$

where

$$I_{m,n}^{s} = \int_{t_n}^{t_n+\delta t} F^{iv}\{(V_b - v_n), t_m\}dt' \cong F^{iv}\{(V_b - v_n), t_m\}\delta t \tag{23}$$

and

$$I_{m,n}^{imp} = \int_{t_n}^{t_n+\delta t} g_l^{imp}(t_m - t')dt' \cong g_l^{imp}(t_m - t_n)\delta t. \tag{24}$$

The voltage coefficients can be obtained, through simple algebraic manipulations, marching on time using the following update rule:

$$v_m = \frac{\sum_{n=-\infty}^{m} V_b I_{m,n}^{s} - \sum_{n=-\infty}^{m-1}\left(v_n I_{m,n}^{s} + I_{m,n}^{imp}\right)}{\left(I_{m,m}^{s} + I_{m,m}^{imp}\right)} \tag{25}$$

with $v_m = 0, \forall m < (t_0/\delta t)$.

The simplest case in which the load can be represented with a resistive load, $R_l = (1/G_l)$, without history implies that the right-hand side of (24) simplifies into $g_l^{imp}(t_m - t_n)\delta t = \delta_{n,m}G_l$, where $\delta_{n,m}$ is the Kronecker delta function. This assumption is well representative for broadband antennas printed on the back of silicon lenses, commonly used in TD THz systems [17].

To clarify the procedure, the voltage and currents in the load prescribed for a specific case representing a PCA are shown in

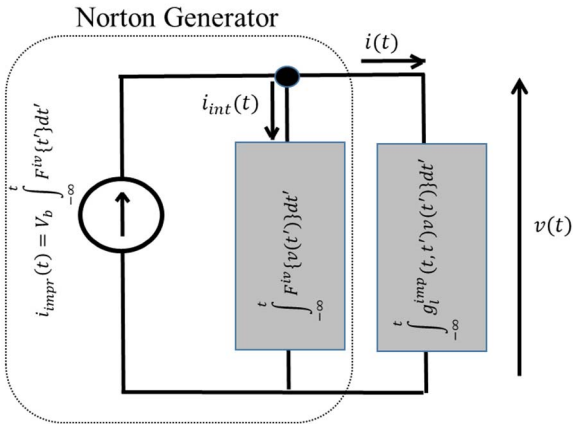

Fig. 8. Equivalent Norton circuit components.

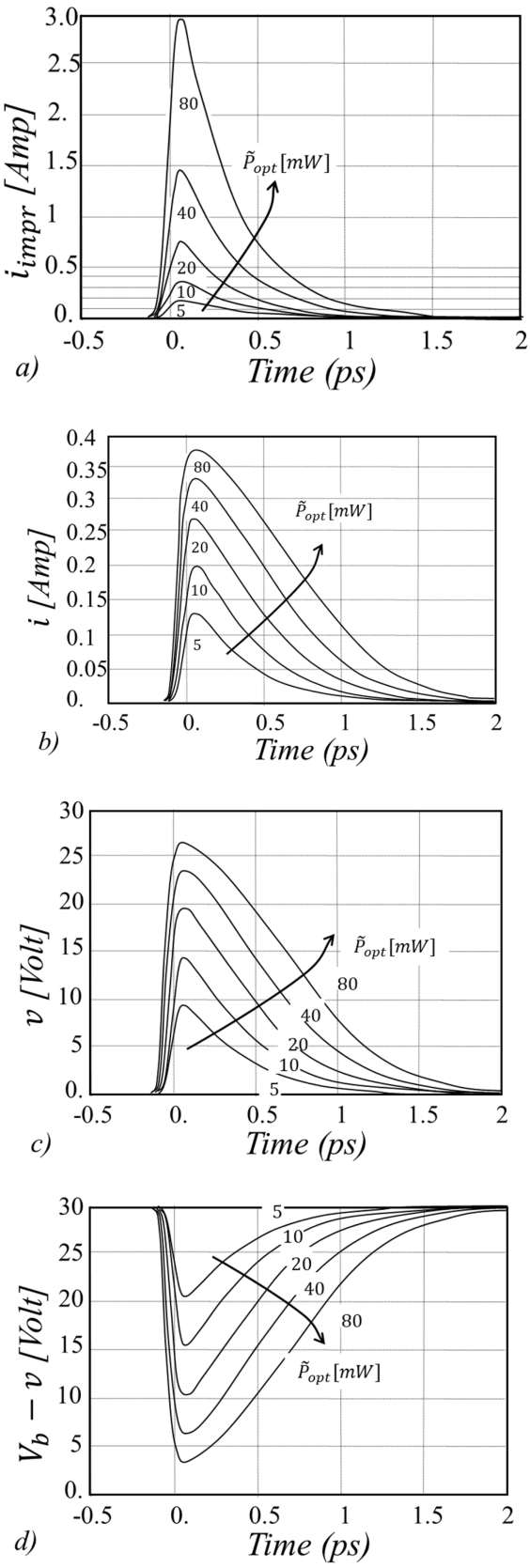

Fig. 9. Time evolutions of voltage and currents circuit of Fig. 8, for increasing optical excitation. (a) Impressed current. (b) Current in the load. (c) Voltage drop across the load. (d) Voltage across the gap.

Fig. 9. This case is taken to be representative for a broadband bow-tie antenna discussed in [13]. Bow ties printed on the back of a silicon lens typically have input radiation resistances that can be approximated as $R_l = 70\ \Omega$ in the targeted THz spectrum and behave as reactive circuits at low frequencies. The PCA source is assumed to be realized with an LT GaAs gap whose cross-sectional area is $\pi a^2 = 20\ \mu\text{m}^2$ and the gap length is $\Delta_z = 10\ \mu$m.

The material is characterized by a scattering time and a recombination time of $\tau_s = 8 \times 10^{-15}$ s and $\tau_c = 0.3 \times 10^{-12}$ s, respectively. The laser pulse is characterized by $\tau_l = 10^{-13}$ s and the average laser power $\tilde{P}_{opt}$, introduced in Section VI, is varied from 4 to 90 mW. Note that this power is the one assumed to be absorbed by the PC gap. The gap is excited with unitary optical efficiency and the pulse is centered in $t_0 = 0$. Furthermore, the gap is biased at voltage $V_b = 30$ V. Fig. 9(a) shows the impressed current, $i_{impr}(t)$, while Fig. 9(b) shows the current in the load, $i(t)$.

One can observe that when the optical excitation of the gap is relatively small, the current in the load is essentially equal to the impressed current, as the internal loading is almost an open circuit. For larger optical power, the impressed current is much higher.

VI. Energy Considerations

To estimate the energy generated in the THz band of interest, it is necessary to consider again (1)–(3) that describe the powers available to the load and dissipated in the gap. Specializing (1) to the case of a resistive load, R_l, the energy provided in correspondence with each laser pulse can be expressed as follows:

$$E_l(R_l) = \int_{t_0 - \frac{\tau_p}{2}}^{t_0+T} p_l(t, R_l)dt \tag{26}$$

where the dependence of the power from the value of the load resistance has been indicated explicitly. The extremes of integration in (26) refer to the time intervals in which the pulses are significantly different from zero (with reference to Fig. 9) and T is the laser pulse repetition period. The average power can be easily obtained as $\tilde{P}_l = (E_l(R_l)/T)$. (Note that the tilde is going to be retained to represent average power in the rest of this two parts article.) Fig. 10 shows the average power in the load for the example in Fig. 9, as a function of the average optical power and assuming a typical period $T = 12.5$ ns. Using the same procedure and (3), the total average power provided by the bias, also shown in Fig. 10, can be obtained by first evaluating the energy per pulse

$$E_{tot}(R_l) = V_b \int_{t_0 - \frac{\tau_p}{2}}^{t_0+T} i(t)dt \tag{27}$$

and then dividing it by the period: $\tilde{P}_{tot} = E_{tot}/T$. Eventually, the actual dissipated power is the difference between the total generated power and the load power: $\tilde{P}_{diss} = \tilde{P}_{tot} - \tilde{P}_l$.

Care should be taken to the role of the generator internal load, in Fig. 8, where $i_{int}(t)$ flows. It is possible to calculate

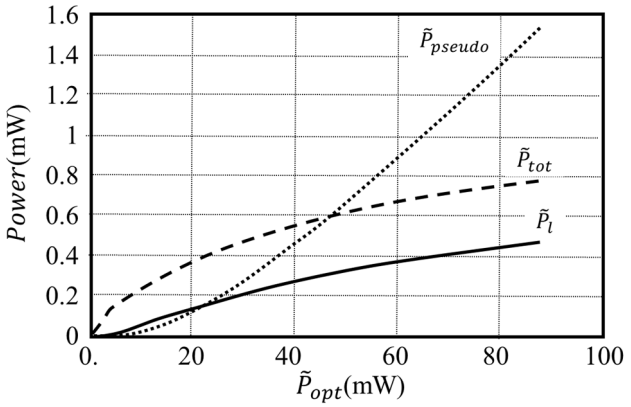

Fig. 10. Average power for the case discussed in Fig. 9 versus the average absorbed laser power. Radiated power (solid), total power (dashed), and pseudo power (dotted).

as auxiliary quantity the pseudo energy dissipated in the generator load as follows:

$$E_{pseudo}(R_l) = \int_{t_0}^{t_0+T} v(t, R_l) i_{int}(t, R_l) dt. \tag{28}$$

The average pseudo power, $\tilde{P}_{pseudo} = E_{pseudo}(R_l)/T$, is also shown in Fig. 10 for sake of completeness. However, we recall that it has no physical significance, and one should not be surprised if it appears to be larger than the total power involved in the radiation mechanism.

As explained in [18, Sec. 12:29]: "It must be emphasized that, as in any Thevenin equivalent circuit, the equivalent circuit was derived to tell what happens in the load under different load conditions, and any significance cannot be automatically attached to a calculation of power loss in the internal impedance of the equivalent circuit." The same, of course, applies to the present Norton circuit, whose derivation is also based on the use of the equivalence theorem.

A. Source Efficiency

The energy that the pulsed PC source can generate is limited by the amplitude of the bias voltage that can be applied before a fatal breakdown of the PC gap. This limitation has little to do with the skills of the designer in optimizing the structures. Nevertheless, it is common to read that PCA sources are very inefficient. This is because of an unfortunate choice for the assumed efficiency parameter. In the THz TD community [11] and antenna community [12], the PCA efficiency η_{pca} is typically related to the ratio between the average THz power delivered to the load, $\tilde{P}_l$, and the average optical power $\tilde{P}_{opt}$ used to activate the transient

$$\eta_{pca} = \frac{\tilde{P}_l}{\tilde{P}_{opt}}. \tag{29}$$

This terminology is taken from photovoltaic (PV) cells. The latter systems present many similarities to the PCA sources. They generate dc energy and are effectively using the optical power as the main source, with typical efficiencies $\eta_{PV} \approx$ 20%–40%. In PV cells, the biasing voltage has a minor role. In the present pulsed THz sources, it is clear that η_{pca}, shown in Fig. 11 for the case of Figs. 9 and 10, is lower than 1%.

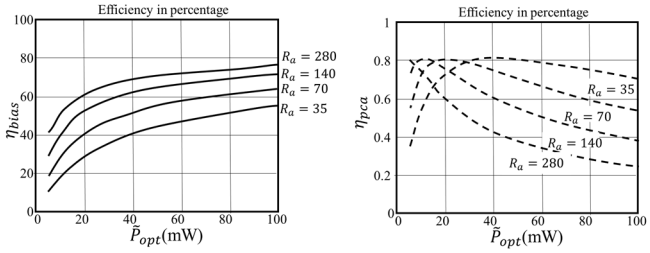

Fig. 11. Bias (solid) and PCA (dashed) efficiencies as a function of the optical average power excitation and for different antenna resistances.

However, for PCA efficiency, the THz power radiated is actually provided by the dc biasing generator. The optical power has only the role, admittedly important, to tune the internal load of the PC source. Accordingly, it could be convenient to introduce a source efficiency related to the biasing voltage defined as follows:

$$\eta_{bias} = \frac{\tilde{P}_l}{\tilde{P}_{tot}}. \tag{30}$$

Fig. 11 shows the biasing efficiency η_{bias} for the case investigated in Fig. 10. The values are between 10% and 70% depending on the optical pump and the resistive load, here indicated as R_a. In our view, this biasing efficiency, η_{bias}, is more suitable for the characterization of PCA efficiency than the standard efficiency η_{pca} as it renders visible what is the possible margin of improvements, on the antenna side for any given design. The main guideline is that the antenna radiation resistance should be as high as possible so that the PCA starts radiating also for low optical excitations. However, since the antennas typically adopted are also required to be broadband, options are limited.

VII. Conclusion

Resorting to the use of the equivalence theorem, this article introduces a TD Norton equivalent circuit to characterize the voltage and current distributions in the load of a pulsed PC THz source. The circuit allows the evaluation of the THz power generated and the energy spectra of the pulses, as well as the ohmic power dissipated in the photoconducting gap. A common assumption in the field of PCA sources is that the key efficiency should relate to the THz power and the optical power. In contrast, we suggest the introduction of a biasing efficiency defined as the ratio between the power generated in the THz spectrum and the total power supplied by the biasing source. The validation of the proposed Norton circuit will be presented in the companion paper [13], with the introduction of the specific constitutive relations of an LT GaAs photoconducting material.

References

[1] D. H. Auston, K. P. Cheung, and P. R. Smith, "Picosecond photoconducting Hertzian dipoles," *Appl. Phys. Lett.*, vol. 45, no. 3, pp. 284–286, May 1984.

[2] D. Grischkowsky, S. Keiding, M. van Exter, and C. Fattinger, "Far-infrared time-domain spectroscopy with terahertz beams of dielectrics and semiconductors," *J. Opt. Soc. Amer. B, Opt. Phys.*, vol. 7, no. 10, pp. 2006–2015, Oct. 1990.

[3] P. U. Jepsen, R. H. Jacobsen, and S. R. Keiding, "Generation and detection of terahertz pulses from biased semiconductor antennas," *J. Opt. Soc. Amer. B, Opt. Phys.*, vol. 13, no. 11, pp. 2424–2436, Nov. 1996.
[4] S. Verghese, K. A. McIntosh, and E. R. Brown, "Highly tunable fiber-coupled photomixers with coherent terahertz output power," *IEEE Trans. Microw. Theory Techn.*, vol. 45, no. 8, pp. 1301–1309, Aug. 1997.
[5] M. Tani, S. Matsuura, K. Sakai, and S. Nakashima, "Emission characteristics of photoconductive antennas based on low-temperature-grown GaAs and semi-insulating GaAs," *Appl. Opt.*, vol. 36, no. 30, pp. 7853–7859, Oct. 1997.
[6] G. C. Loata, M. D. Thomson, T. Löffler, and H. G. Roskos, "Radiation field screening in photoconductive antennae studied via pulsed terahertz emission spectroscopy," *Appl. Phys. Lett.*, vol. 91, Dec. 2007, Art. no. 232506.
[7] O. A. Castañeda-Uribe, C. A. Criollo, S. Winnerl, M. Helm, and A. Avila, "Comparative study of equivalent circuit models for photoconductive antennas," *Opt. Exp.*, vol. 26, no. 22, pp. 29017–29031, 2018.
[8] A. Garufo, G. Carluccio, N. Llombart, and A. Neto, "Norton equivalent circuit for pulsed photoconductive antennas–Part I: Theoretical model," *IEEE Trans. Antennas Propag.*, vol. 66, no. 4, pp. 1635–1645, Apr. 2018.
[9] A. Garufo *et al.*, "A connected array of coherent photoconductive pulsed sources to generate mW average power in the submillimeter wavelength band," *IEEE Trans. Terahertz Sci. Technol.*, vol. 9, no. 3, pp. 221–236, May 2019.
[10] M. Silverberg and O. Wing, "Time domain computer solutions for networks containing lumped nonlinear elements," *IEEE Trans. Circuit Theory*, vol. 15, no. 3, pp. 292–294, Sep. 1968.
[11] D. Sin and D. S. Citrin, "Coulomb and radiation screening in photo conductive THz sources," *Appl. Phys. Lett.*, vol. 88, Jan. 2006, Art. no. 161117.
[12] N. Khiabani, Y. Huang, Y.-C. Shen, and S. J. Boyes, "Theoretical modeling of a photoconductive antenna in a terahertz pulsed system," *IEEE Trans. Antennas Propag.*, vol. 61, no. 4, pp. 1538–1546, Apr. 2013, doi: 10.1109/TAP.2013.2239599.
[13] A. Fiorellini Bernardis, P. M. Sberna, J. Bueno, H. Zhang, N. Llombart, and A. Neto, "Time-domain modelling of pulsed photoconducting sources—Part II: Characterization of an LT GaAs bow-tie antenna," *Trans. Antennas Propag.*, vol. 71, no. 3, pp. 2536–2545, Mar. 2023.
[14] T. Wang, R. F. Harrington, and J. R. Mautz, "Electromagnetic scattering from and transmission through arbitrary apertures in conducting bodies," *IEEE Trans. Antennas Propag.*, vol. 38, no. 11, pp. 1805–1814, Nov. 1990, doi: 10.1109/8.102743.
[15] J. Van Bladel, "The matrix formulation of scattering problems," *IEEE Trans. Microw. Theory Techn.*, vol. 14, no. 3, pp. 130–135, Mar. 1966.
[16] J. Shan and T. F. Heinz, "Terahertz radiation from semiconductors," in *Ultrafast Dynamical Processes in Semiconductors*, vol. 92, K.-T. Tsen, Ed. Berlin, Germany: Springer-Verlag, 2004, pp. 1–59.
[17] N. Llombart and A. Neto, "THz time-domain sensing: The antenna dispersion problem and a possible solution," *IEEE Trans. Terahertz Sci. Technol.*, vol. 2, no. 4, pp. 416–423, Jul. 2012.
[18] S. Ramo and J. R. Whinnery, *Fields and Waves in Modern Radio*, 2nd ed. New York, NY, USA: Wiley, 1959.

Andrea Neto (Fellow, IEEE) received the Laurea degree *(summa cum laude)* in electronic engineering from the University of Florence, Florence, Italy, in 1994, and the Ph.D. degree in electromagnetics from the University of Siena, Siena, Italy, in 2000. Part of his Ph.D. degree was developed at the European Space Agency Research and Technology Center, Noordwijk, The Netherlands, where he focused on the Antenna Section for over two years.

From 2000 to 2001, he was a Post-Doctoral Researcher with the California Institute of Technology, Pasadena, CA, USA, where he was with the Sub-Millimeter Wave Advanced Technology Group. From 2002 to January 2010, he was a Senior Antenna Scientist with TNO Defence, Security and Safety, The Hague, The Netherlands. In February 2010, he became a Full Professor of applied electromagnetism with the Electrical Engineering, Mathematics and Computer Science (EEMCS) Department, Technical University of Delft, Delft, The Netherlands, where he formed and leads the THz Sensing Group. His current research interests include analysis and design of antennas with an emphasis on arrays, dielectric lens antennas, wideband antennas, EBG structures, and terahertz (THz) antennas.

Dr. Neto is currently a member of the Technical Board of the European School of Antennas and an Organizer of the course on THz Antennas and Imaging techniques. In 2011, he was a recipient of the European Research Council (ERC) Consolidator Grant to perform research on Advanced Antenna Architectures for THz Sensing Systems, the H. A. Wheeler Award for the Best Applications Paper of 2008 in the IEEE TRANSACTIONS ON ANTENNAS AND PROPAGATION, the Best Innovative Paper Prize of the 30th ESA Antenna Workshop in 2008, and the Best Antenna Theory Paper Prize of the European Conference on Antennas and Propagation (EuCAP) in 2010. He has served as an Associate Editor for the IEEE TRANSACTIONS ON ANTENNAS AND PROPAGATION, IEEE ANTENNAS AND WIRELESS PROPAGATION LETTERS, and the IEEE TRANSACTIONS ON TERAHERTZ SCIENCE AND TECHNOLOGY. He served as a Co-Chair for the Technical Program Committee for the conferences Eucap 2021 and IRMMW-THZ 2022.

Nuria Llombart Juan (Fellow, IEEE) received the degree in electrical engineering and the Ph.D. degree from the Polytechnic University of Valencia, Valencia, Spain, in 2002 and 2006, respectively.

From 2002 to 2007, she was a Researcher with the Antenna Group, TNO Defence, Security and Safety Institute, The Hague, The Netherlands. From 2007 to 2010, she was a Post-Doctoral Fellow with the Sub-Millimeter Wave Advance Technology Group, Jet Propulsion Laboratory, California Institute of Technology, Pasadena, CA, USA. She was a Ramón y Cajal Fellow with the Optics Department, Complutense University of Madrid, Madrid, Spain, from 2010 to 2012. In 2012, she joined the THz Sensing Group, Delft University of Technology, Delft, The Netherlands, where she is currently an Associate Professor. She has coauthored over 100 journals and international conference contributions. Her current research interests include analysis and design of planar antennas, periodic structures, reflector antennas, lens antennas, and waveguide structures, with an emphasis on the terahertz (THz) range.

Dr. Llombart Juan is a Board Member of the IRMMW-THz International Society. She was a co-recipient of the H. A. Wheeler Award for the Best Applications Paper in the IEEE TRANSACTIONS ON ANTENNAS AND PROPAGATION in 2008, the 2014 THz Science and Technology Best Paper Award of the IEEE Microwave Theory and Techniques Society, and several NASA awards. She received the 2014 IEEE Antenna and Propagation Society Lot Shafai Mid-Career Distinguished Achievement Award. She serves as a Topical Editor for the IEEE TRANSACTIONS ON TERAHERTZ SCIENCE AND TECHNOLOGY, the IEEE ANTENNAS AND WIRELESS PROPAGATION LETTERS, and the Antenna Applications Corner of the *IEEE Antennas and Propagation Magazine*. She is the Chair of the IRMMW-THz Conference held in Delft in 2022.

Angelo Freni (Senior Member, IEEE) received the Laurea degree in electronics engineering from the University of Florence, Florence, Italy, in 1987.

Since 1990, he has been an Assistant Professor with the Department of Electronic Engineering, University of Florence, where he has been an Associate Professor of electromagnetism, since 2002. In 1994, he joined the Department of Engineering, University of Cambridge, Cambridge, U.K., where he was involved in research and concerning the extension and the application of the finite-element method to the electromagnetic scattering from periodic structures. From 2009 to 2010, he spent one year as a Researcher at the Defense, Security and Safety Institute, Netherlands Organization for Applied Scientific Research (TNO), Hague, The Netherlands, focused on the electromagnetic modeling of kinetic inductance devices and their coupling with array of slots in terahertz range. Since 2012, he has been a Visiting Professor with the TU Delft University of Technology, Delft, The Netherlands. From 1995 to 1999, he was an Adjunct Professor with the University of Pisa, Pisa, Italy. In 2014, he obtained the Full Professor qualification. His current research interests include meteorological radar systems, radiowave propagation, numerical and asymptotic methods in electromagnetic scattering and antenna problems, electromagnetic interaction with moving media, and remote sensing. In particular, part of his research concerned numerical techniques based on the integral equation, with a focus on domain-decomposition and fast solution methods.